INTERNATIONAL JOURNAL FOR NUMERICAL METHODS IN FLUIDS, VOL. 20, 233–253 (1995)

COMPARISON OF VARIANTS OF THE BI-CONJUGATE GRADIENT METHOD FOR COMPRESSIBLE NAVIER–STOKES SOLVER WITH SECOND-MOMENT CLOSURE

C. C. CHUANG* AND C. C. CHIENG†‡

* *Department of Power Mechanical Engineering,* † *Department of Nuclear Engineering*
National Tsing Hua University, Hsinchu, Taiwan 30043, Republic of China

SUMMARY

Variants of the bi-conjugate gradient (Bi-CG) method are used to resolve the problem of slow convergence in CFD when it is applied to complex flow field simulation using higher-order turbulence models. In this study the Navier–Stokes and Reynolds stress transport equations are discretized with an implicit, total variation diminishing (TVD), finite volume formulation. The preconditioning technique of incomplete lower–upper (ILU) factorization is incorporated into the conjugate gradient square (CGS), bi-conjugate gradient stable (Bi-CGSTAB) and transpose-free quasi-minimal residual (TFQMR) algorithms to accelerate convergence of the overall itertive methods. Computations have been carried out for separated flow fields over transonic bumps, supersonic bases and supersonic compression corners. By comparisons of the convergence rate with each other and with the conventional approximate factorization (AF) method it is shown that the Bi-CGSTAB method gives the most efficient convergence rate among these methods and can speed up the CPU time by a factor of 2·4–6·5 as compared with the AF method. Moreover, the AF method may yield somewhat different results from variants of the Bi-CG method owing to the factorization error which introduces a higher level of convergence criterion.

KEYWORDS Bi-conjugate gradient method Second moment turbulent closure compressible Separated flow Convergence behaviour

1. INTRODUCTION

With increasing computer power and continuing algorithm development, computational fluid dynamics (CFD) has recently made remarkable progress for high-speed flows. The solution of the compressible Navier–Stokes equations with higher-order turbulence closure models is of fundamental importance for a wide variety of flows. In particular, turbulent separated flows are currently of great interest because the capability of accurately predicting flow separation plays an important role in evaluating the performance of aerodynamic design. Over the years the approximate factorization (AF)[1] technique has been widely used to solve the implicitly discretized Navier–Stokes equations and turbulent transport equations. However, good convergence behaviour for the system of these equations is difficult to achieve when higher-order turbulence model closures such as the two-equation model, algebraic Reynolds stress model and differential Reynolds stress model are employed, because stiffness may arise especially near the wall owing to the use of a very fine mesh. The slow convergence problem in the AF method may be caused by the existence of a factorization error which is introduced during

‡ Author to whom correspondence should be addressed.

CCC 0271–2091/95/030233–21

Received February 1994
Revised August 1994

factorizing of the two-dimensional operator into two one-dimensional operators. Moreover, most investigators must give special attention to finding good initial guesses of mean flow fields and turbulent properties to reach acceptable convergence. Therefore an efficient and robust numerical solver for complex flow simulation using higher-order turbulence models is necessary to get a fast convergence rate and reliable results even when no special effort for initial conditions is required.

Recently the generalized conjugate gradient methods have been demonstrated to greatly improve the robustness and convergence in current CFD applications.[2,3] Among these generalized conjugate gradient methods, the CGS[4] (conjugate gradient square) method, which removes the matrix transpose computation, has been recognized as an attractive iterative method because it is competitive with GMRES[5] (generalized minimal residual) in convergence rate and is economical in both storage requirements and computing time. However, in some applications the CGS method could face an irregular convergence behaviour close to the final solution and spoil the numerical result. Therfore more smoothly converging variants of BI-CGSTAB[6] (bi-conjugate gradient stable) and TFQMR[7] (transpose-free quasi-minimal residual) algorithms have been developed and employed in the computations. Moreover, it is also found that the preconditioning technique is critical to the success of generalized CG methods, and preconditioned conjugate gradient and its generalizations have been successfully applied in the CFD codes of Venkatakrishnan[8] for subsonic and transonic flows and Ajmani *et al.*[9] for transonic and hypersonic flows. However, only the Baldwin–Lomax algebraic turbulence model is incorporated in their studies.

More recently Lin *et al.*[10] have achieved a good convergence rate by the use of these variants of the Bi-CG method with an ILU preconditioner[11] for turbulent, transonic, separated flow using the k–ε two-equation model with uniform distributions of the mean flow variables and turbulent properties as the initial guesses. However, the k–ε model is limited to applications of complex flow field prediction such as shock-induced separation and supersonic base flow. The present study extends the work of Lin *et al.* by the use of second-moment turbulent closure for transonic and supersonic separated flow fields. In this paper, transonic flow over a bump,[12,13] supersonic flow over a compression corner[14,15] and supersonic flow behind a missile-type afterbody[16,17] are the test cases computed with the implicit TVD scheme and Shima's near-wall Reynolds stress model (RSM)[18] to demonstrate the superiority of CGS, Bi-CGSTAB and TFQMR algorithms over the AF method in both computational efficiency and accuracy. Moreover, a comparison between the computed surface pressure distributions and the experimental data will be presented to show the improvement of the RSM model over the two-equation model for separated flow field simulations.

2. PHYSICAL AND MATHEMATICAL MODELS

The governing equations used to describe the mean flow in this study are the time-dependent, mass averaged Navier–Stokes equations for a compressible fluid. Depending on the turbulence models used, the equations are augmentd by additional equations. In the present application, turbulence closure is described by Shima's near-wall Reynolds stress model,[18] so that it involves four transport equations for the independent stresses $\overline{u_i'u_j'}$ and a fifth transport equation for the turbulent energy dissipation rate ε. The Navier–Stokes equation and turbulent transport equations for two-dimensional or axisymmetric flow can be written in vector form in an arbitrary co-ordinate system (ξ, η) as

$$\partial_t(\hat{Q}) + \partial_\xi(\hat{E} - \hat{E}_v) + \partial_\eta(\hat{F} - \hat{F}_v) + j(\hat{H} - \hat{H}_v) = \hat{W}. \tag{1}$$

The equation describes two-dimensional flow if $j = 0$ and axisymmetric flow if $j = 1$. $\hat{Q}$ is the vector of dependent variables, $\hat{Q} = Q/J = J^{-1}\{\rho, \rho u, \rho v, E_t, \rho\overline{u'u'}, \rho\overline{v'v'}, \rho\overline{w'w'}, \rho\overline{u'v'}, \rho\varepsilon\}$, in the application of second-moment turbulent closure. The vectors $\hat{E}$ and $\hat{F}$ represent the corresponding convective

fluxes and contain convection and pressure terms, while the vectors $\hat{E}_V$ and $\hat{F}_V$ describe diffusive fluxes in the ξ- and η-directions respectively. The vectors $\hat{H}$ and $\hat{H}_V$ are the source terms of convection, diffusion and turbulent energy associated with axisymmetric co-ordinates, while $\hat{W}$ contains the source terms for production, destruction and redistribution of turbulent energy. J is the Jacobian and the perfect gas equation of state is added to complete the system of equations.

The Reynolds stress components $\overline{u_i'u_j'}$ are computed from the transport equations of Reynolds stresses ($\overline{u_i'u_j'}$) and the dissipation rate of turbulent kinetic energy (ε). These equations can be expressed as

$$\begin{aligned}
\frac{\partial(\rho\overline{u_i'u_j'})}{\partial t}+\frac{\partial(\rho U_k\overline{u_i'u_j'})}{\partial x_k} &= C_{s1}\frac{\partial[(k/\varepsilon)\overline{u_k'u_l'}\partial(\overline{u_i'u_j'})/\partial x_l]}{\partial x_k}+P_{ij}+E_{ij}+\phi_{ij}+\phi_{ij,w}\\
\frac{\partial(\rho\varepsilon)}{\partial t}+\frac{\partial(\rho U_k\varepsilon)}{\partial x_k} &= C_\varepsilon\frac{\partial[(k/\varepsilon)\overline{u_k'u_l'}\partial\varepsilon/\partial x_l]}{\partial x_k}+\frac{C_{\varepsilon1}(1+C_{\varepsilon4}f_w)P\varepsilon}{k}-\frac{C_{\varepsilon2}f_\varepsilon\rho\varepsilon\bar{\varepsilon}}{k}+\xi_{SH}
\end{aligned} \tag{2}$$

so that the source terms of $\hat{W}$ in the turbulent transport equations of the Reynolds stress model can be expressed as

$$\begin{aligned}
\hat{W}_{\overline{u_i'u_j'}} &= P_{ij}+E_{ij}+\phi_{ij}+\phi_{ij,w},\\
\hat{W}_\varepsilon &= C_{\varepsilon1}(1+C_{\varepsilon4}f_w)P\varepsilon/k-C_{\varepsilon2}f_\varepsilon\rho\varepsilon\bar{\varepsilon}/k+\xi_{SH}.
\end{aligned} \tag{3}$$

The detailed expressions of the Reynolds stress generation rate P_{ij}, viscous dissipation rate E_{ij} and pressure/strain-related redistribution ϕ_{ij} as well as $\phi_{ij,w}$ in Shima's Reynolds stress model are available in Reference 18. The inclusion of the high anisotropic effect of the turbulent stresses in the immediate vicinity of the wall and the easy assessment of the empirical constants for the pressure/strain term are the reasons for choosing Shima's Reynolds stress model for this study.

3. NUMERICAL METHODS

Using the finite volume formulation, the governing equation (1) can be implicitly discretized as

$$\begin{aligned}
(\Delta Q)_{i,j}^n=\hat{Q}_{i,j}^{n+1}-\hat{Q}_{i,j}^n=&-\frac{\Delta t}{\Delta\xi}[(\tilde{E}-\tilde{E}_v)_{i+1/2,j}-(\tilde{E}-\tilde{E}_v)_{i-1/2,j}]^{n+1}\\
&-\frac{\Delta t}{\Delta\eta}[(\tilde{F}-\tilde{F}_v)_{i,j+1/2}-(\tilde{F}-\tilde{F}_v)_{i,j-1/2}]^{n+1}+\Delta t\hat{W}_{i,j}^n-j\Delta t(\hat{H}-\hat{H}_v)_{i,j}^n.
\end{aligned} \tag{4}$$

In the present study Yee and Harten's TVD scheme[19] is applied for the convective flux terms $(\tilde{E},\tilde{F})$, while the viscous flux terms $(\tilde{E}_v,\tilde{F}_v)$ are evaluated with the central difference approximation.

The RHS of equation (4) is linearized in time about the nth time level in the computations. This transforms equation (4) into a system of linear, simultaneous algebraic equations which can be solved in several ways. In this paper the AF method and variants of the Bi-CG method such as CGS, Bi-CGSTAB and TFQMR are selected to make a comparison of computational efficiency. Brief descriptions of the methods are given below.

3.1. AF method

The implicit, approximately factored method for the full Navier–Stokes equations and Reynolds stress transport equations using upwind differencing in the ξ- and η-directions can be written in the form

$$[I + \Delta t(\partial_\xi^- \hat{A}^+ + \partial_\xi^+ \hat{A}^-)]^n [I + \Delta t(\partial_\eta^- \hat{B}^+ + \partial_\eta^+ \hat{B}^-) - \Delta t\hat{D}]^n (\Delta\hat{Q})_{i,j}^n = \text{RHS of (4) at the } n\text{th time level}, \tag{5}$$

where $\hat{A}^+, \hat{A}^-$ and $\hat{B}^+, \hat{B}^-$ are the positive and negative split Jacobian matrices in the ξ- and η-directions respectively. The additional matrix $\hat{D}$ is used for higher-order turbulence models to overcome the stiffness problem caused by the use of a very fine mesh near the wall, where the source term $\hat{W}$ could be very large. The value of $\hat{D}$ is set to be the maximum value of the partial derivatives of the source terms $\hat{W}_{\rho\overline{u_i'u_j'}}$ and $\hat{W}_{\rho\varepsilon}$ with respect to the conservation of variables $\rho\overline{u_i'u_j'}$ and $\rho\varepsilon$ respectively. In the present study the mean flow equations and Reynolds stress transport equations are decoupled in the computation so that the work of solving a 9×9 block tridiagonal matrix equation can now be reduced to solve a 4×4 block tridiagonal matrix equation and five tridiagonal matrix equations. Because a factorization error is introduced in this scheme during factorizing of the two-dimensional operator to two one-dimensional operators, the allowable time step is limited and a relaxation factor of 0·10–0·25 must be added in the computation of the Reynolds stress transport equations for the sake of stability.

3.2. Preconditioned iterative method

The factored matrix equation (5) can be replaced by the non-factored form

$$\tilde{A}_{i,j}(\Delta Q)_{i-1,j} + \tilde{C}_{i,j}(\Delta Q)_{i+1,j} + \tilde{E}_{i,j}(\Delta Q)_{i,j-1} + \tilde{F}_{i,j}(\Delta Q)_{i,j+1} + \tilde{D}_{i,j}(\Delta Q)_{i,j} = \tilde{B}_{i,j}, \tag{6}$$

where

$$\begin{aligned}
\tilde{B}_{i,j} &= [\text{RHS of (5)}]/\text{Vol}_{i,j},\\
\tilde{A}_{i,j} &= -(\Delta t/\text{Vol}_{i,j})\hat{A}_{i-1/2,j}^+,\\
\tilde{C}_{i,j} &= -(\Delta t/\text{Vol}_{i,j})\hat{A}_{i+1/2,j}^-,\\
\tilde{E}_{i,j} &= -(\Delta t/\text{Vol}_{i,j})\hat{B}_{i,j-1/2}^+,\\
\tilde{F}_{i,j} &= -(\Delta t/\text{Vol}_{i,j})\hat{B}_{i,j+1/2}^-,\\
\tilde{D}_{i,j} &= (\Delta t/\text{Vol}_{i,j})(\hat{A}_{i+1/2,j}^+ - \hat{A}_{i-1/2,j}^- + \hat{B}_{i,j+1/2}^+ - \hat{B}_{i,j-1/2}^-) + I + (\Delta t)D_{i,j}.
\end{aligned}$$

Equation (6) forms a diagonally dominant, block pentadiagonal matrix system equation $Ax = b$. The coefficient matrices $\tilde{A}_{i,j}, \tilde{C}_{i,j}, \tilde{D}_{i,j}, \tilde{E}_{i,j}$ and $\tilde{F}_{i,j}$ are 9×9 square matrices and the right-hand-side matrix $\tilde{B}_{i,j}$ is a 9×1 vector. The unknown $(\Delta Q)_{i,j}$ is conventionally evaluated by the block Gauss–Seidel method[20,21] but the convergence rate is very slow. In recent years generalized conjugate gradient methods such as Bi-CG have become powerful iterative schems for solving the linear system $Ax = b$ with general non-symmetric, non-singular coefficient matrices. For the Bi-CG method[22] the approximations are constructed in such a way that the residual r_j is orthogonal to another vector row $\hat{r}_0, \hat{r}_1, \ldots, \hat{r}_{j-1}$ and vice versa. This can be accomplished by two three-term recurrence relations for rows $\{r_j\}$ and $\{\hat{r}_j\}$, and the residual vectors of the Bi-CG algorithm can be written as $r_n = P_n(A)r_0$ and $\hat{r}_n = P_n(A^T)\hat{r}_0$ respectively, where P_n is a polynomial of degree less than or equal to n. However, the Bi-

CG method is very cumbersome to programme, because the computational work of the Bi-CG algorithm is twice that of the CG algorithm and it requires the computation of A^T.

Sonneveld[4] observed that only the convergence of $\{r_n\}$ is exploited in the case of convergence. He suggested the CGS method where the polynomial $p_n(A)$ is applied twice, i.e. $\tilde{r}_n = p_n^2(A)r_0$, as the residuals to estimate x_n of the solution. Then the process to generate the sequence of r_n is no longer needed and multiplications by the matrix A^T are avoided. In many situations, however, one is faced with a somewhat irregular convergence behaviour of CGS, in particular when starting the iteration close to the solution. To smooth the convergence history without losing the attractive convergence speed of CGS, Van der Vorst[6] proposed an apparently rather stable and more efficient scheme called Bi-CGSTAB in which the residual $r_n = Q_n(A)p_n(A)r_0$ is developed. The polynomial $Q_n(A)$ is of the form $Q_n(A) = (1 - \omega_1 A)(1 - \omega_2 A) \ldots (1 - \omega_n A)$, where $\omega_1, \omega_2, \ldots, \omega_n$ are selected by minimizing r_n with respect to ω_n.

However, CGS and Bi-CGSTAB methods are all derived from Bi-CG method and the residual norm is not characterized by a minimization property, which means that the algorithms could exhibit a rather irregular convergence behaviour with wild oscillations in the residual norm. Based on the look-ahead Lanczos approach, Freund and Nathtigal[23] proposed a variant Bi-CG method, the quasi-minimal residual (QMR) method, which remedies the convergence problems of Bi-CG, but both Bi-CG and QMR require matrix multiplications by A^T. More recently Freund [7] proposed the TFQMR method which is defined by a quasi-minimization of the residual norm, but similarly to the CGS algorithms, it does not require multiplications by A^T. He showed that the resulting TFQMR method can be easily implemented and can remedy the irregular convergence behaviour with wild oscillations in the residual norm of Bi-CG-like methods.

Meanwhile, the convergence rate of conjugate gradient methods depends strongly on the eigenvalue distribution of the coefficient matrix. Instead of solving the original linear system $Ax = b$, in application a preconditioned technique is used to solve the related linear system $K^{-1}Ax = K^{-1}b$. The matrix product $K^{-1}A$ has a more favourable eigenspectrum distribution than A has, i.e. the eigenvalues are more clustered near unity. The choice of preconditioner in the present study is based on an incomplete line LU factorization of the matrix A (denoted as ILU), which consists of a strictly block lower triangular matrix of A (denoted as L), a strictly block upper triangular matrix of A (denoted as U) and a non-zero block diagonal matrix D, satisfying $A = (L + D)D^{-1}(U + D) + E$, where E is the deviation matrix. The preconditioning with ILU is done by choosing $K = (L + D_i)D_i^{-1}(U + D_i)$, where D_i is slightly modified from D, and the solution procedure is available in Reference 11. The algorithms for solving $K^{-1}Ax = K^{-1}b$ by the preconditioning CGS, Bi-CGSTAB and TFQMR methods are described briefly below.

Preconditioning CGS method

Give an initial guess x_0, $r_0 = b - Ax_0$;
Choose a vector $\hat{r}_0$ such that $(r_0, \hat{r}_0) \neq 0$, e.g. $\hat{r}_0 = r_0$;
let $\rho_0 = (\hat{r}_0, r_0)$, $p_0 = q_0 = r_0$;
do $k = 0, 1, \ldots$ until residual $<$ tolerance
Solve y from $Ky = p_k$;
$v = Ay$
$\alpha_k = \rho_k/(\hat{r}_0, v)$;
$s = q_k - \alpha_k v$
$t = q_k + s$
Solve z from $Kz = t$;
$x_{k+1} = x_k + \alpha_k z$;

$u = Az$
$r_{k+1} = r_k - \alpha u;$
$\rho_{k+1} = (r_0, r_{k+1})$
$\beta_k = \rho_{k+1}/\rho_k;$
$q_{k+1} = r_{k+1} + \beta_k s$
$p_{k+1} = q_{k+1} + \beta_k(\beta_k p_k + s);$

Preconditioning Bi-CGSTAB method

Give an initial guess x_0, $r_0 = b - Ax_0$;
Choose a vector $\hat{r}_0$ such that $(r_0, \hat{r}_0) \neq 0$, e.g. $\hat{r}_0 = r_0$;
let $\rho_0 = (\hat{r}_0, r_0)$, $p_0 = r_0$;
do $k = 0, 1, \ldots$ until residual $<$ tolerance
Solve y from $Ky = p_k$;
$v = Ay$
$\alpha_k = \rho_k/(\hat{r}_0, v);$
$s = r_k - \alpha_k v$
Solve z from $Kz = s$;
$t = Az$
$\omega_k = (s, t)/(t, t)$
$r_{k+1} = s - \omega_k t$
$x_{k+1} = x_k + \alpha_k y + \omega_k z$
$\rho_{k+1} = (r_0, r_{k+1})$
$\beta_k = (\alpha_k/\omega_k)\ (\rho_{k+1}/\rho_k);$
$p_{k+1} = r_{k+1} + \beta_k(p_k - \omega_k v);$

Preconditioning TFQMR method

Given an initial guess x_0, $r_0 = b - Ax_0$;
Choose a vector $\hat{r}_0$ such that $(r_0, \hat{r}_0) \neq 0$, e.g. $\hat{r}_0 = r_0$;
let $\rho_0 = (\hat{r}_0, r_0)$, $p_0 = q_0 = r_0$, $d_0 = 0$, $\theta_0 = 0$, $\tau_0 = \omega_1 = \|r_0\|$;
do $k = 0, 1, \ldots$ until residual $<$ tolerance
$y = Ap_k$
Solve v from $Kv = y$;
$\alpha_k = \rho_k/(\hat{r}_0, v);$
$u_k = q_k - \alpha_k v$
$s = q_k + u_k$
$t = As$
Solve w from $Kw = t$;
$r_{k+1} = r_k - \alpha_k w$
$\omega_{m+1} = \sqrt{(\|r_{k+1}\|\|r_k\|)}$ if $m = 2k + 1$
$\omega_{m+1} = \|r_{k+1}\|$ if $m = 2k + 2$
$\theta_m = \omega_{m+1}/\tau_{m-1}$
$c_m = 1/\sqrt{(1 + \theta_m\theta_m)}$
$\tau_m = \tau_{m-1}\theta_m c_m$
$d_m = c_m^2\ \alpha_k y_m + c_m^2\theta_{m-1}^2 d_{m-1}$
$y_m = q_k$ if $m = 2k + 1$
$y_m = u_k$ if $m = 2k + 2$
$x_m = x_{m-1} + d_m$

$\rho_{k+1} = (\hat{r}_0, r_{k+1});$
$\beta_k = \rho_{k+1}/\rho_k;$
$q_{k+1} = r_{k+1} + \beta_k u_k$
$p_{k+1} = q_{k+1} + \beta_k(\beta_\kappa p_k + u_k);$

It can be seen that both CGS and Bi-CGSTAB produce only one iterate x_n per iteration, while TFQMR generates two iterates x_m with indices $m = 2k + 1$ and $2k + 2$ in the kth step of the interation.

4. INITIAL AND BOUNDARY CONDITIONS

A uniform flow field with uniformly distributed turbulence intensity is first assumed to start the computation. The initial conditions of turbulence intensity are set as

$$(\overline{u_1'u_1'})_0 = (\overline{u_2'u_2'})_0 = (\overline{u_3'u_3'})_0 = (\overline{u_1'u_2'})_0 = (0{\cdot}02u_\infty)^2, \qquad \varepsilon_0 = k_0^{3/2}/L, \qquad k_0 = 0{\cdot}5(\overline{u_i'u_i'})_0,$$

where u_∞ is the freestream speed and L is the characteristic mixing length.

The boundary conditions are set as follows. (1) The characteristic extrapolation technique is applied at the far-field ($\eta = \eta_{\max}$) and outflow boundaries, while a zeroth-order extrapolation is used to specify the conditions at the symmetric boundary. (2) No-slip boundary conditions for velocities are adopted on the solid surface, which is assumed to be an adiabatic wall. (3) The density and pressure on the wall are set equal to the values at the node points next to the wall. (4) For the Reynolds stress ($\overline{u_i'u_j'}$) and turbulent kinetic dissipation rate (ε) calculations a zeroth-order extrapolation is used to specify the conditions at the outflow and symmetric boundaries, except that the value of $\overline{u_1'u_2'}$ is set to zero at the symmetric boundary. The values of $\overline{u_i'u_j'}$ are set to zero at the solid wall. However, the value of ε at the wall is finite and equal to $\nu\partial^2 k/\partial x_\ell \partial x_\ell$ in Shima's near-wall Reynolds stress model.

It is noted that the computations are performed with the Reynolds stress model from the first time step and no 'pre-run' is necessary in the present study. However, other authors[24,25] perform the computations with the algebraic turbulence model until an acceptably converged solution is obtained and then continue the computations with higher-order turbulence models for a certain number of time steps.

5. RESULTS AND DISCUSSION

This study investigates the improvement in the convergence behaviour of variants of the Bi-CG method when the Reynolds stress model is incorporated into the simulation of compressible separated flow fields. The following cases are chosen here to illustrate the scope of the study and its outcome: (1) transonic shock-induced separated flow over an axisymmetric bump[12,13] ($M_\infty = 0{\cdot}875$, $Re_\infty = 1{\cdot}36 \times 10^7\ \mathrm{m}^{-1}$); (2) supersonic separated flow over 20°[14] ($M_\infty = 2{\cdot}79$, $Re_\infty = 6{\cdot}60 \times 10^7\ \mathrm{m}^{-1}$) and 24°[14,15] ($M_\infty = 2{\cdot}85$, $Re_\infty = 6{\cdot}30 \times 10^7\ \mathrm{m}^{-1}$) compression corners; (3) supersonic base flow behind a missile-type afterbody[16,17] ($M_\infty = 2{\cdot}45$, $Re_\infty = 15{\cdot}9 \times 10^7\ \mathrm{m}^{-1}$). The first and second examples have their focus on strong shock wave/boundary layer interaction. The last case examines the base drag prediction which is very important in the aerodynamics of unpowered flight. In these cases comparisons with experimental data are also performed and the comparisons of convergence rate are based on the maximum possible Courant number according to the stability restriction. In the present computations only one iteration of solving (6) by the variants of the Bi-CG method is used for each time step, because only the approximated solution is required at each time step in the time-marching problem. The tolerance levels for the cases of bump, compression corner and supersonic base are about 10^{-6}, 10^{-5} and 10^{-3} respectively.

5.1. *Transonic shock-induced separated flow over axisymmetric bump*

The first test case is the axisymmetric, transonic, shock wave/boundary layer experiment of Bachalo and Johnson.[12,13] A schematic diagram of the axisymmetric bump is shown in Figure 1 along with the grid system. The circular arc bump has a thickness of 1·91 cm and a chord length C of 20·32 cm and is affixed to a thin-walled cylinder of outer diameter 15·2 cm. Its leading edge is joined to the cylinder by a smooth circular arc of radius 18·3 cm which is tangent to the cylinder at 3·33 cm upstream and to the bump at 2·05 cm downstream of the intersection of the bump arc with the cylinder. Here a strong shock impinging on the bump induces a separated flow region similar to that developed on an aerofoil. In previous studies many computations based on various turbulence closure models have been performed, e.g. algebraic turbulence models,[26,27] a higher-order turbulence model of the k–ε two-equation model[10] as well as the algebraic stress model.[28] However, further improved results are desired for the predictions of shock location and flowfields around the separation region due to the shock/boundary layer interaction when k–ε or ASM turbulence models are employed.

The grid system used in the numerical computations is a 150 × 71 H-type grid with 60 points behind its trailing edge and clustering near the shock location and at the wall to ensure high resolution of the shock region and viscous sublayer, which corresponds to a minimum y^+ of 0·5. The boundaries of the computational domain are extended 4·5C in the normal direction and from $-4C$ to $4C$ in the flow direction.

Figure 2 shows the computed and measured pressure distributions along the bump surface. The characteristic features of shock position and pressure level in the shock wave/boundary layer interaction region are much better predicted by the RSM model than by the k–ε two-equation model.[10] It is also noted that the pressure distribution obtained by the AF method is slightly different from that yielded by the three variants of the Bi-CG method in the recirculation region. This difference could be caused by the factorization error of the AF method, which introduces a higher level of convergence criteria in the turbulent transport equations. Figure 3 shows the Mach number contours obtained by the Bi-CGSTAB and AF methods. Because the computational results are the same among the three

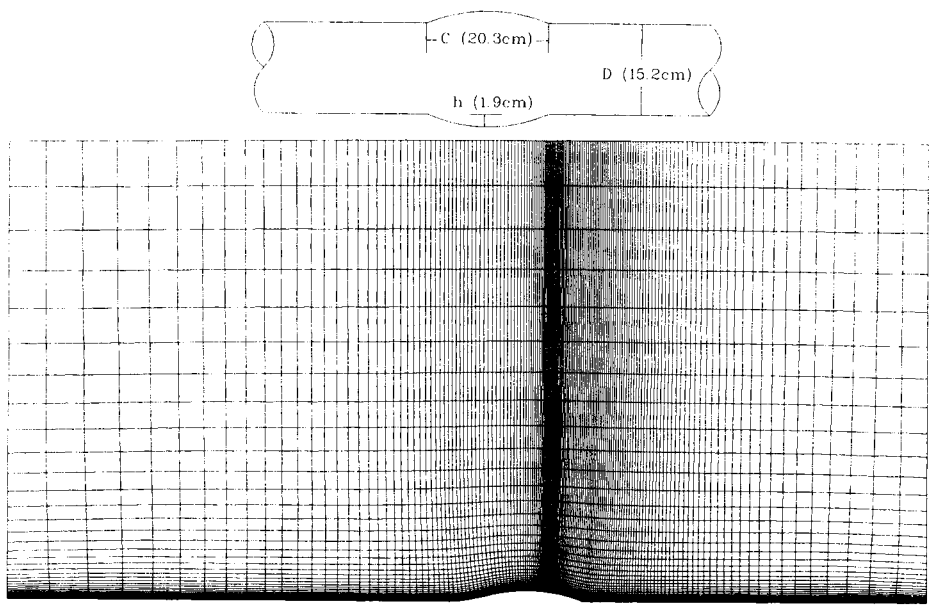

Figure 1. A 150 × 71 hyperbolic H-type grid (bump)

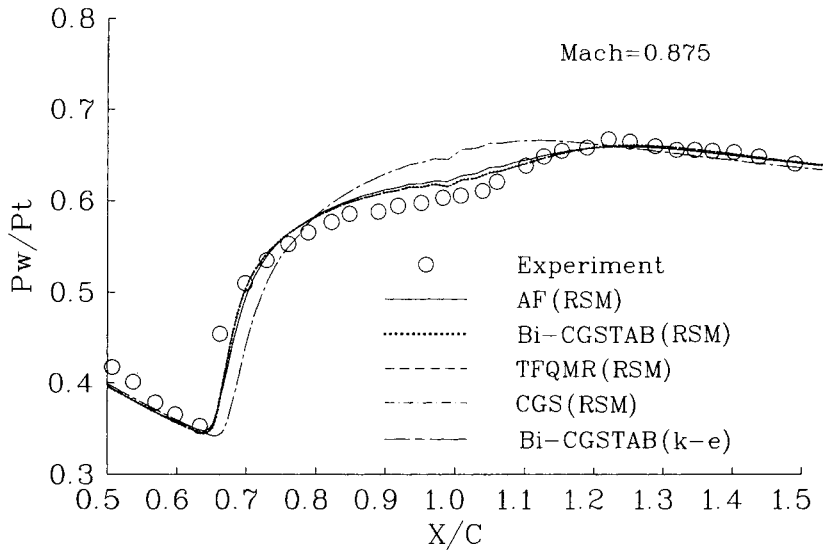

Figure 2. Surface pressure distributions for various solvers and turbulence models (bump)

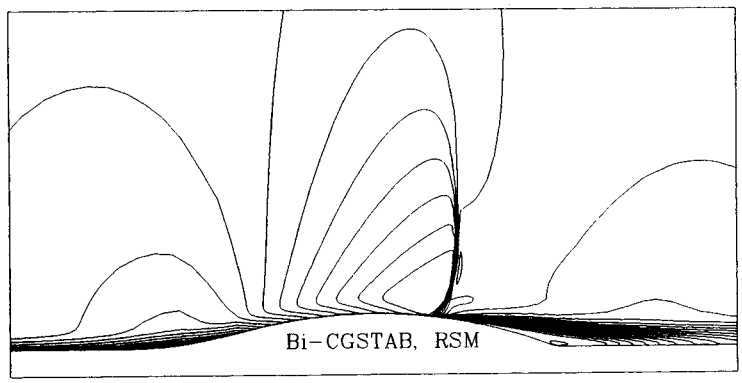

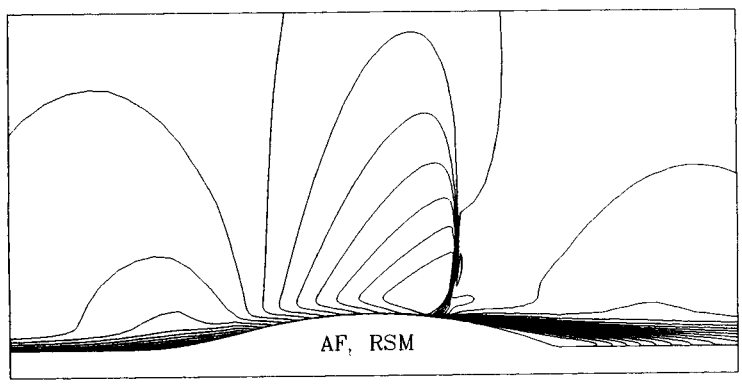

Figure 3. Mach number contours for various solvers (bump)

variants of the Bi-CG method, only the contour of the Bi-CGSTAB method is plotted for comparison with that of the AF method. The Bi-CGSTAB algorithm in particular gives a somewhat higher resolution for the prediction of shock wave/boundary layer interaction than the AF algorithm does.

The convergence histories of the L_2 and maximum energy residuals by various implicit solvers are plotted in Figure 4. The L_2 residual defined as the square root of $\sum_i^N [(\Delta V \Delta\rho/\Delta t)_i^2 + (\Delta V\ \Delta\rho u/\Delta t)_i^2 + (\Delta V\ \Delta\rho v/\Delta t)_i^2 + (\Delta V\ \Delta E_t/\Delta t)_i^2]/N$, displays the overall convergence properties of the flow fields, where ΔV is the differential volume of the ith computational cell and N is the total number of computational cells. The maximum energy residual indicates the local convergence behaviour of the flowfields and is defined as the maximum of $[(E_t^{n+1} - E_t^n)/\Delta t]_i$, where i is the index of the computational cell, E_t is the total energy and n is the iteration time. The time step by the AF method is 0·6 and the relaxation factors for $\overline{u_i' u_j'}$ and ε are 0·15 during the iteration steps. However, the maximum possible time steps by the three variants of the Bi-CG method, i.e. CGS, Bi-CGSTAB and TFQMR, are 3·0, 3·3 and 3·3 respectively and no relaxation is necessary for the turbulent transport equations of $\overline{u_i' u_j'}$ and ε. The L_2 residual can only be reduced in an oscillatory manner to about 10^{-8} after 12,000 iteration steps by the AF method, but fewer than 4000 iteration steps are needed by the three variants of the Bi-CG method to achieve the same performance. The irregular and oscillatory convergence characteristics of these schemes could be caused by the strongly non-linear properties of the turbulence model. The CPU times of each iteration are 3·74, 5·75, 5·71 and 6·97 s for the AF, CGS, Bi-CGSTAB and TFQMR methods respectively when the computations are performed on an HP-9000/735 scalar workstation. The computing efficiency, defined as the CPU time per iteration per grid point, and related parameters for these four methods are summarized in Table I. Generally speaking, the use of the Bi-CGSTAB method leads to a speed-up of the CPU time by a factor of about 2·4 as compared with the use of the AF method to achieve the same convergence criterion. Among the three variant Bi-CG methods, TFQMR and Bi-CGSTAB are slightly better than CGS in terms of the convergence rate, but TFQMR consumes more CPU time per iteration than the other two methods.

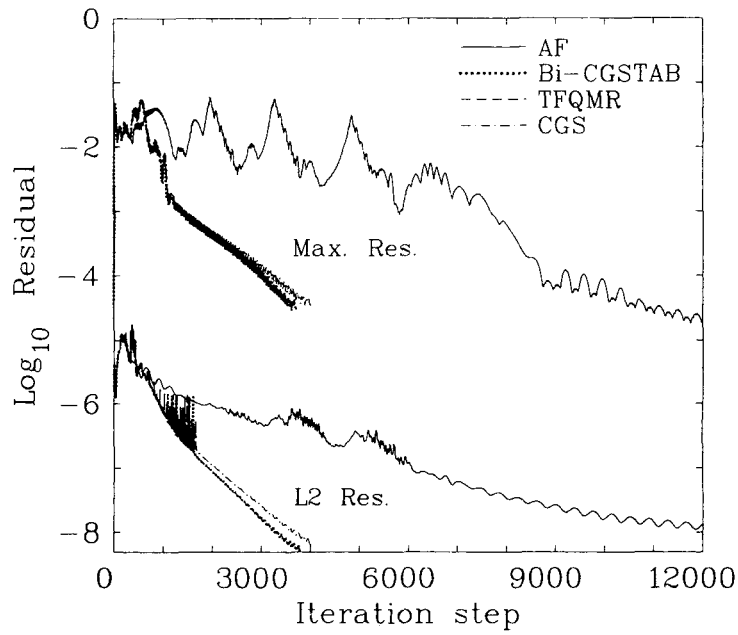

Figure 4. Convergence histories of L_2 and maximum energy residuals (bump)

Table I. Computing efficiency (CPU seconds per iteration per grid point on an HP-9000/735 workstation) and related parameters for various solvers

		AF	CGS	BI-CGSTAB	TFQMR
	Computing efficiency	3.51×10^{-4}	5.40×10^{-4}	5.36×10^{-4}	6.54×10^{-4}
Bump	CPU seconds*	44880	20125	18843	2300
	Max. time step size	0.6	3.0	3.3	3.3
	Iteration no.*	12000	3500	3300	3300
20° ramp	CPU seconds*	67800	15630	15540	18960
	Max. time step size	0.2	1.6	1.8	1.8
	Iteration no.*	20000	3000	3000	3000
Base	CPU seconds*	91200	22624	14060	23996
	Max. time step size	0.2	1.5	1.8	2.4
	Iteration no.*	20000	3200	2000	2800

* The numbers are for the L_2 residual down to three orders lower.

5.2. *Supersonic flow over compression corner*

This problem shows that an oblique shock impinging on the boundary layer ahead of the corner of a 20° ($M_\infty = 2{\cdot}79$) or 24° ($M_\infty = 2{\cdot}85$) ramp[14,15] induces a massive separated flow region owing to the upstream influence. The primary objective is to demonstrate the performance of variants of the Bi-CG method for stronger, supersonic shock wave/boundary layer interactions of various extents, so a comparison of the 20° and 24° ramps is made here.

The 136 × 71 H-type grid systems used in the computation of these two cases are shown in Figures 5 and 6. The grid systems are clustered near the corner and at the wall surface, corresponding to a minimum y^+ of 0·7 to resolve the steep variation in flow fields across the viscous layer where viscous–inviscid interaction occurs. The upper boundary is placed about $9\delta_0$ away from the wall and the outer boundary is lcoated at $8\delta_0$ downstream of the corner, where δ_0 is the measured boundary layer thickness. The measured inflow velocity profiles are set at positions $X = -1{\cdot}6\delta_0$ and $-2{\cdot}17\delta_0$ for the 20° and 24° ramps respectively.

Figure 7 shows a comparison of surface pressure distributions along the 20° ramp. It is noted that the Reynolds stress turbulence model solved by the variants of the Bi-CG method can well predict the initial pressure rise but overestimates the extent of the upstream influence indicated by the plateau in the experimental pressure distribution. However, the AF method reaches a different solution owing to the factorization error in this scheme. The surface pressure distribution over the 24° ramp is computed and compared with data by Horstman *et al.*[14] and Dolling and Murphy[15] and the prediction associated with the Jones–Launder two-equation model by Coakley and Huang[29] in Figure 8. Numerous computations using two-equation turbulence models have also been made for this case and further improvements in predictions of the upstream influence, the wall pressure rise through separation and the pressure under the separated shear layer are desired.[29] However, the pressure distribution predicted by the present Reynolds stress model follows the data of Dolling and Murphy and the trend is similar to the results in Reference 30. The agreement between computation and experiment shows the improvement achieved with the Reynolds stress model. The difference between the AF method and the variant Bi-CG methods could be due to the factorization error in the AF scheme, which prevents the residual level from converging to satisfactory values. Owing to the higher residual level of the AF method, the solutions obtained by this method may not be good enough when it is applied to simulate complex flow fields using higher-order turbulence models.

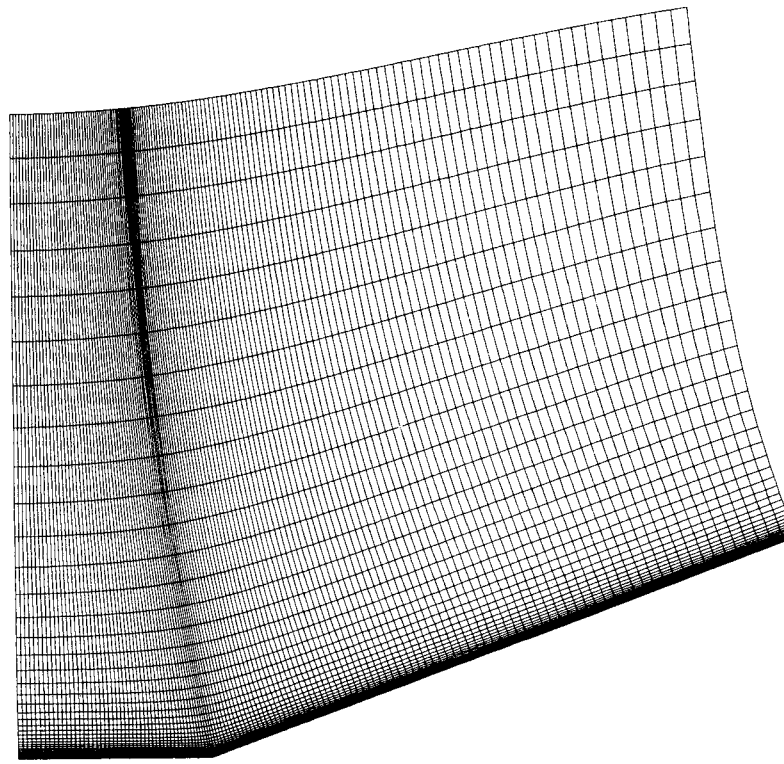

Figure 5. A 136 × 71 hyperbolic H-type grid (20° ramp)

The convergence histories of the L_2 and maximum energy residuals for the 20° ramp by the AF, CGS, TFQMR and Bi-CGSTAB methods are compared in Figure 9. the L_2 and maximum energy residuals are reduced by six orders of magnitude after 38,000 iteration steps when the AF method is employed, but the L_2 and maximum energy residuals can be reduced to the same criterion by the three variants of the Bi-CG method in less than 5500 iteration steps. The maximum possible time steps by the AF, CGS, Bi-CGSTAB and TFQMR methods are 0·2, 1·6, 1·8 and 1·8 respectively and an underrelaxation factor of 0·15 is needed when the AF method is employed. Using the variants of the Bi-CG method, a flattened convergence history is observed during the first 3000 iteration steps to form the oblique shock and then the L_2 and maximum energy residuals converge smoothly and fast to 10^{-9} and 10^{-6} respectively during the 4800th–5500th iteration steps. When the computations are performed on an HP-9000/735 scalar workstation, the CPU times needed for the AF, CGS, TFQMR and Bi-CGSTAB methods are 3·39, 5·21, 6·32 and 5·18 s respectively for each time step. This means that the use of the Bi-CGSATB method could speed up the CPU time by a factor of 4·4 as compared with the use of the AF method to achieve the same convergence criterion. Figure 10 compares the convergence histories of the L_2 and maximum energy residuals for the 24° ramp. In general, Figures 9 and 10 show similar convergence characteristics. However, the allowable maximum time step of the AF method for the 24° ramp (Δt = 0·25) is larger than for the 20° ramp (Δt = 0·2), so that fewer iteration time steps are needed to get a converged result for an oblique shock. Because the extent of separation for the 24° ramp is greater than for the 20° ramp, this increases the convective effects and allows a larger time step for the 24° ramp. The CPU time can be speeded up by a factor of 4·1 by the use of the Bi-CGSTAB method as compared with the AF method to achieve the same convergence criterion.

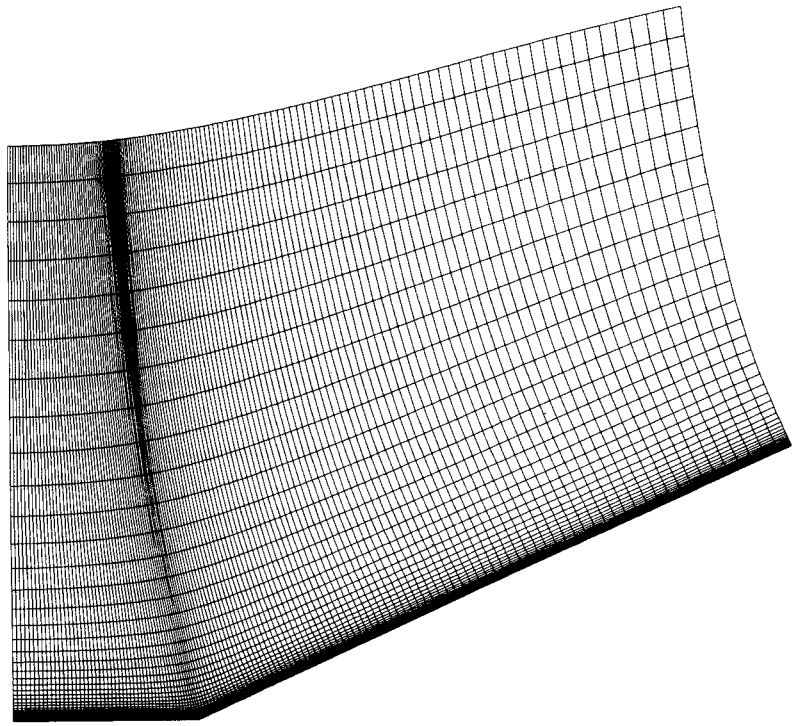

Figure 6. A 136 × 71 hyperbolic H-type grid (24° ramp)

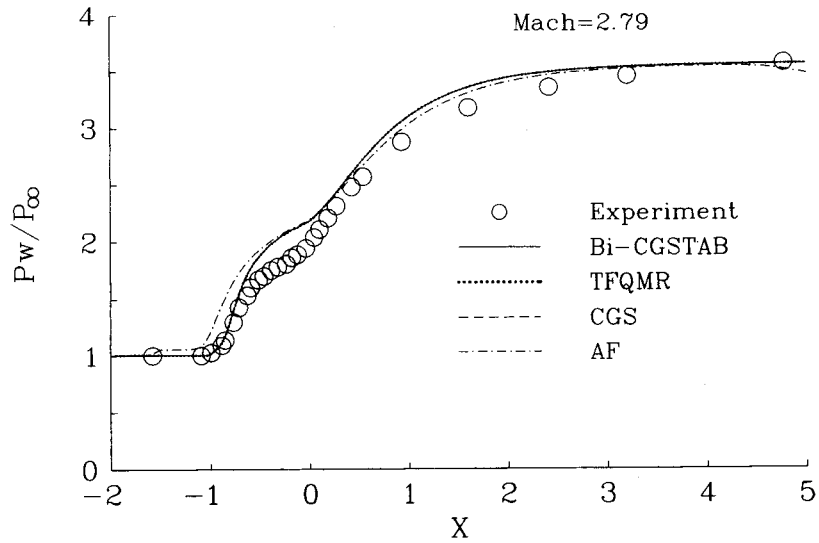

Figure 7. Surface pressure distributions for various solvers (20° ramp)

Figure 11 shows the convergence histories of the Reynolds stress components $\overline{u'u'}$ and $\overline{v'v'}$ solved by the AF and Bi-CGSTAB methods for the 20° ramp. Although the L_2 residual of the AF and Bi-CGSTAB methods could reduce to the same convergence criterion (Figure 9), the turbulent transport equations are converged to different residual levels and this influences the surface pressure distributions of the two solvers as shown in Figure 7. Owing to the factorization error in the AF scheme, the

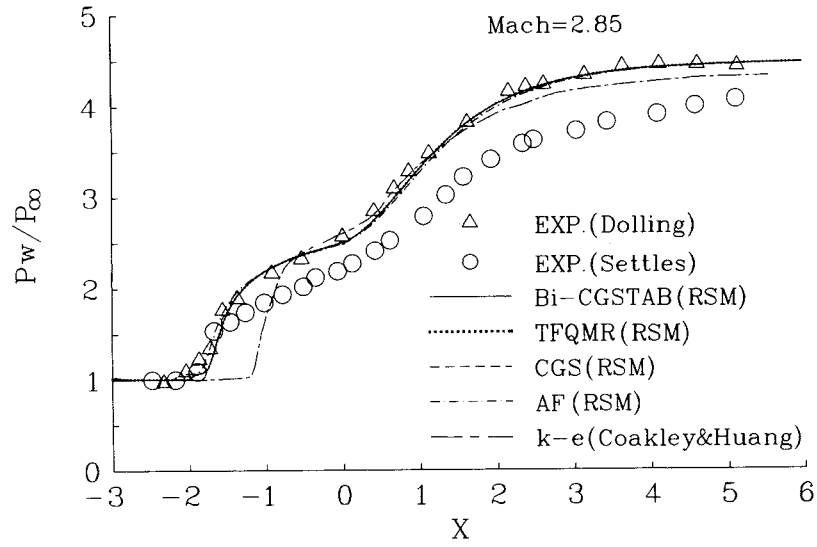

Figure 8. Surface pressure distributions for various solvers and turbulence models (24° ramp)

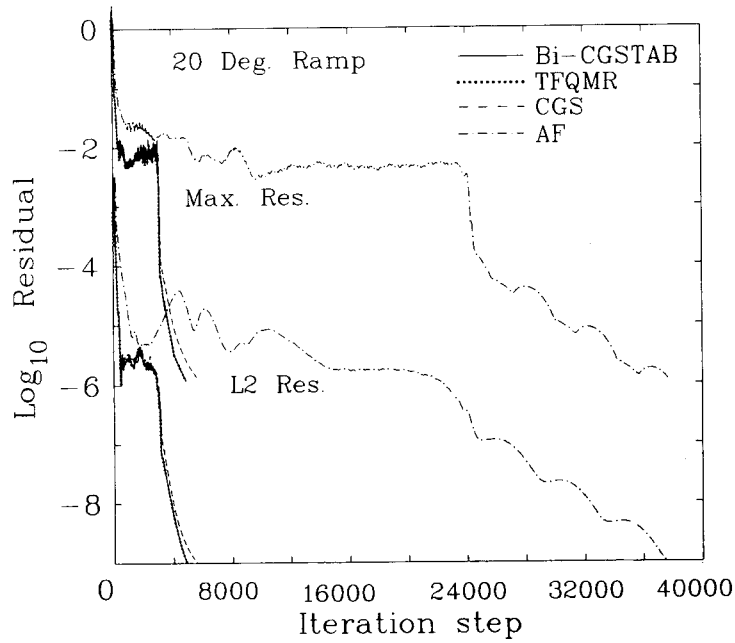

Figure 9. Convergence histories of L_2 and maximum energy residuals (20° ramp)

maximum residual levels of the $\overline{u'u'}$ and $\overline{v'v'}$ transport equations by the AF scheme are only reduced to 10^{-4}–10^{-5}; however, the Bi-CGSTAB method reduces the residual levels to 10^{-7}–10^{-8} and achieves a much better convergence criterion. Figure 12 shows the convergence histories of the Reynolds stress components $\overline{w'w'}$ and $\overline{u'v'}$ solved by the AF and Bi-CGSTAB methods for the same case. The Bi-CGSTAB method can reduce the residual level of $\overline{w'w'}$ to a better convergence criterion than the AF

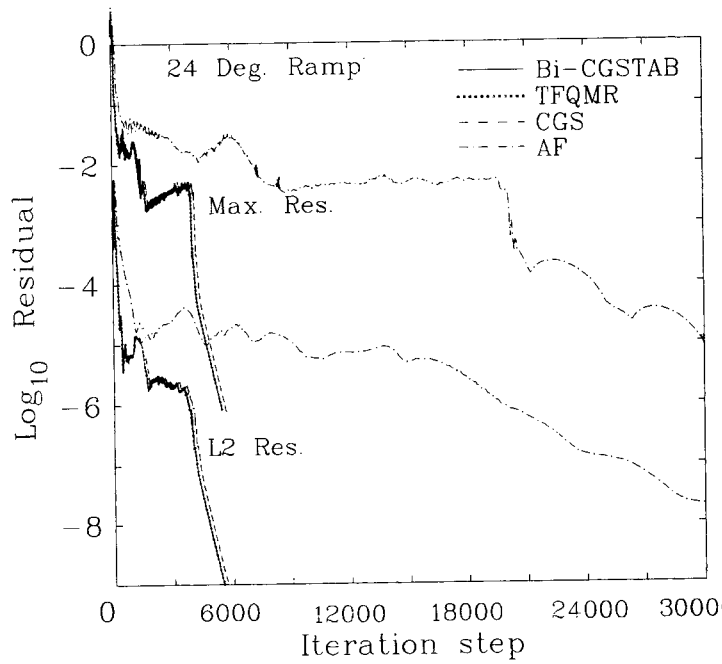

Figure 10. Convergence histories of L_2 and maximum energy residuals (24° ramp)

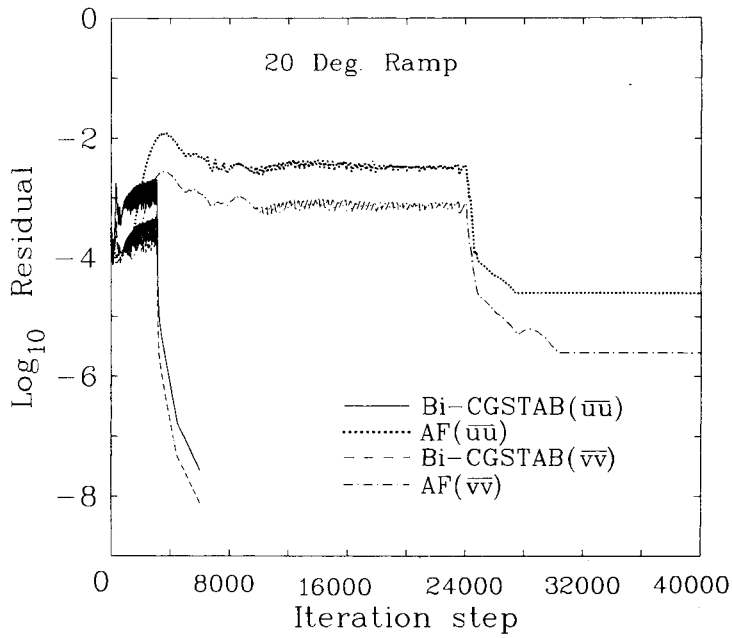

Figure 11. Convergence histories of $\overline{u'u'}$ and $\overline{v'v'}$ residuals (20° ramp)

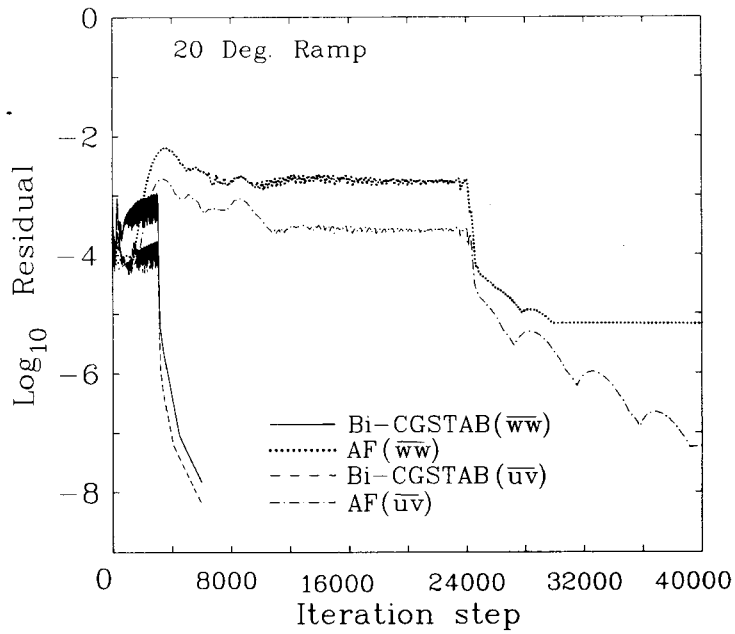

Figure 12. Convergence histories of $\overline{u'u'}$ and $\overline{u'v'}$ residuals (20° ramp)

scheme; however, the residual levels of $\overline{u'v'}$ by both the AF and Bi-CGSTAB methods reach the same convergence criterion.

It is concluded that the factorization error in the AF scheme not only limits the allowable time step, but also the residual levels in the turbulent normal stress transport equations cannot be reduced to low enough values. The unsatisfactory convergence characteristics of the AF method may induce some error when it is applied to simulate complex flow fields using higher-order turbulence models.

5.3. Supersonic base flow behind missile-type afterbody

Base pressure is one of the most important and complicated problems in fluid dynamics and makes a major contribution to the drag of missiles in power-off flight. However, very few quantitative data existed until recently, when Herrin and Dutton published a set of detailed experimental data for the near-wake flow field in axisymmetric supersonic flow.[17] In the present computation the grid system (Figure 13) is a 118 × 111 H-type grid with 55 points on the base surface and clustering in the reversed flow region and shear layer to resolve the steep flow field variation. The outer boundaries in the streamwise and radial directions are 10 calibres away from the base surface and 5·5 calibres away from the axisymmetric axis respectively. Also, the measured inflow velocity profile is set at the corner.

Figure 14 compares the calculated base pressure distributions with the experimental data set of Herrin and Duttan and includes a sketch of the mean flow field structure. This figure shows that the base pressure distributions predicted by the three variant Bi-CG methods and AF method with the Reynolds stress turbulence model are in fairly good agreement with experiment. The conventional k–ε two-equation turbulence model gives the largest variation in base pressure distribution.[31] The base drag coefficients C_{pb} in the present computation by the Reynolds stress and k–ε models are $-0{\cdot}1082$ and $-0{\cdot}1378$ respectively and the result for the RSM is much closer to the measured C_{pb} of $-0{\cdot}102$. This indicates the successful use of the Reynolds stress model for base flow prediction. Figure 15 shows the Mach number contours of measurement and numerical predictions. At the corner the expansion fan can

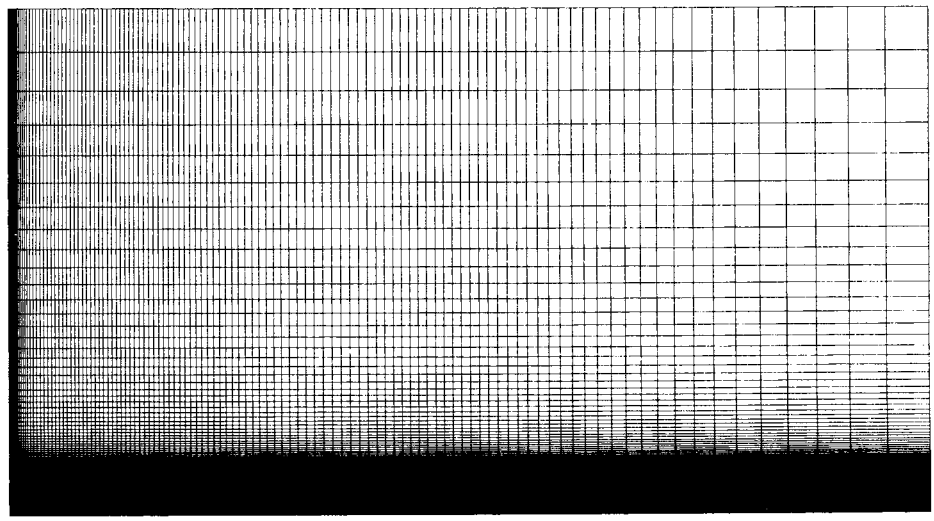

Figure 13. A 118 × 111 hyperbolic H-type grid (supersonic base)

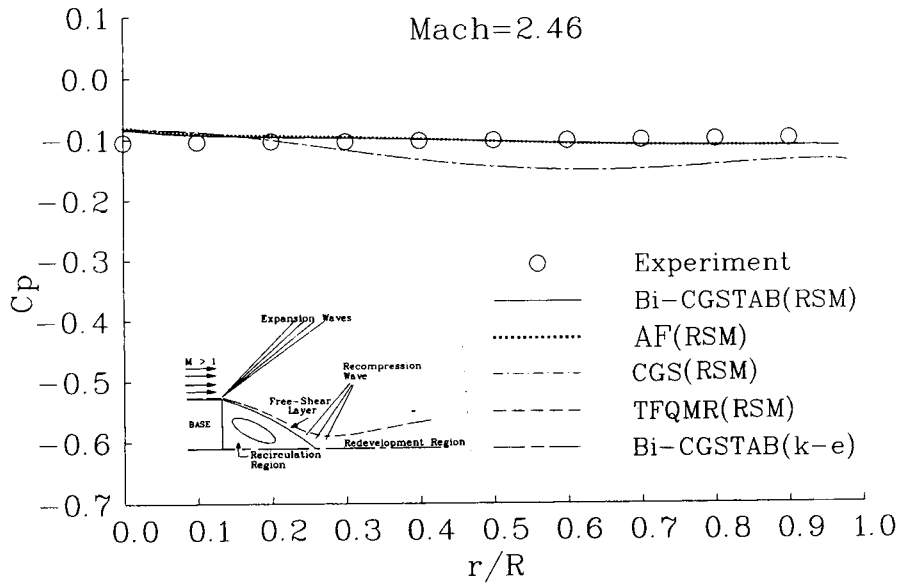

Figure 14. Surface pressure distributions for various solvers and turbulence models (supersonic base)

be recognized by the increasing Mach number, followed by a gradually recompression in the outer flow with decreasing Mach number, as can be seen in the upper right corner of the figures. Comparison of the plots indicates that the factorization error in the AF method somewhat influences the reverse flow region as compared with the Bi-CGSTAB method. In the reverse flow region near the base surface the AF method gives a slightly uniform distribution of Mach number away from the asixymmetric axis.

Figure 16 presents the convergence histories of the L_2 and maximum energy residuals by the AF, CGS, TFQMR and Bi-CGSTAB methods. In the problem of supersonic base flow the L_2 and

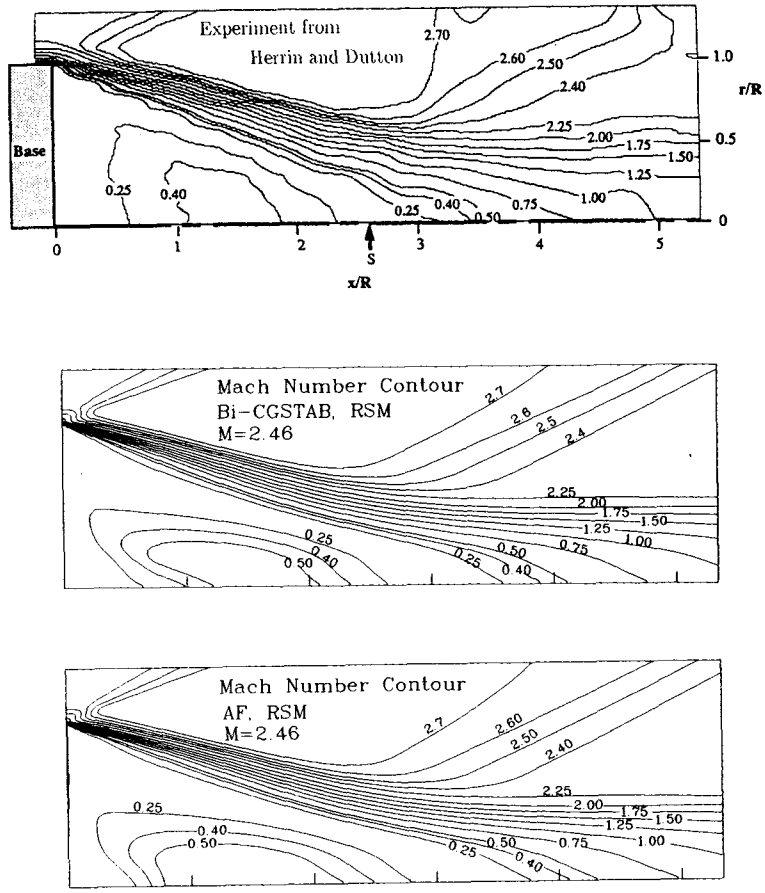

Figure 15. Mach number contours for various solvers (supersonic base)

maximum energy residuals by the AF method are only reduced by about 4·5 and 3 orders of magnitude respectively after 30,000 iteration steps. However, the L_2 and maximum energy residuals can be reduced about 5 and 4 orders of magnitude respectively in only 4000–6000 iteration steps using the three variants of the Bi-CG method. The maximum possible time steps by the AF, CGS, TFQMR and Bi-CGSTAB methods are 0·2, 1·5, 1·8 and 2·4 respectively and it is noted that an underrelaxation factor of 0·20 is needed when the AF method is employed. Among the variant Bi-CG methods, the Bi-CGSTAB method has demonstrated much more stable properties and accepts a larger time step than the CGS and TFQMR methods in the simulation of complex base flow fields. When the computations are performed on an HP-9000/735 scalar workstation, the CPU times needed for the AF, CGS, TFQMR and Bi-CGSTAB methods are 4·56, 7·07, 8·57 and 7·03 respectively for each time step. This means that the use of the Bi-CGSTAB method could speed up the CPU time by a factor of 6·5 as compared with the AF method to achieve the same convergence criterion.

6. CONCLUSIONS

Three variants of the preconditioned bi-conjugate gradient method have been successfully implemented in compressible Navier–Stokes solvers with the Reynolds stress turbulence model and

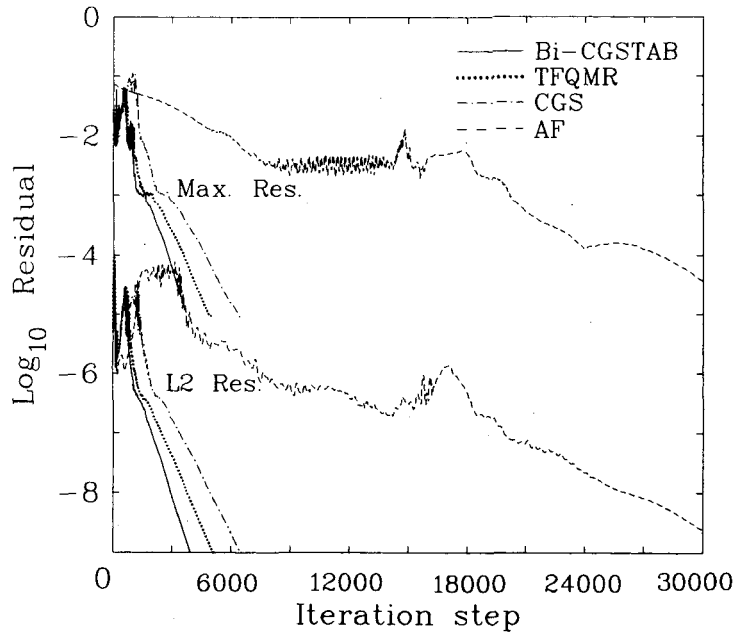

Figure 16. Convergence histories of L_2 and maximum energy residuals (supersonic base)

their efficiencies in the simulation of transonic and supersonic separated flows have been demonstrated. Several conclusions regarding the present study can be made as follows.

(1) Among the three variants of the Bi-CG method, the Bi-CGSTAB method is the most stable one and accepts a larger time step than the CGS and TFQMR methods in the simulation of complex base flow fields.
(2) The factorization error in the AF scheme not only limits the allowable time step but also induces higher levels of residuals in the turbulent transport equations. An error may be induced in solutions owing to the unsatisfactory convergence criterion of the AF method when it is applied to simulate complex flow fields using higher-order turbulence models. Therefore the variants of the Bi-CG method are more effective than the AF method for more complex flow fields.
(3) The numerical implementation of variants of the Bi-CG method makes the computation of complex flow fields with the Reynolds stress turbulence model practical and feasible regarding the CPU requirements and desired accuracy.
(4) The Reynolds stress model provides much better prediction and agreement with experimental data than the k–ε two-equation model for simulations of the complex interactions between shocks and boundary layers.

ACKNOWLEDGEMENTS

The authors want to thank Dr. H. Lin of CSIST at Lung-Tan, Taiwan for his valuable discussions and suggestions regarding the use of variant Bi-CG solvers. They also want to thank the National Science Council of the Republic of China for its support under the contract NSC-82-0413-E-007-109.

APPENDIX: NOMENCLATURE

C_{pb}	dimensionless base drag coefficient, $C_{pb} = 2(P_b - P_\infty)/\gamma M_\infty^2 P_\infty$
$\hat{E}, \hat{F}$	flux vectors in transformed co-ordinates ξ and η
$\hat{E}_v, \hat{F}_v$	viscous flux vectors in transformed co-ordinates
$\hat{H}, \hat{H}_v$	source terms associated with axisymmetric co-ordinates
J	Jacobian
k	turbulent kinetic energy
M	Mach number
P	production rate of turbulent kinetic energy
$\hat{Q}$	vector of dependent variables
Re_∞	Reynolds number ($U_\infty D/\nu$)
R_y	turbulent Reynolds number ($Re_\infty \rho \sqrt{k}\, y_n/\mu_l/M_\infty$)
t	time
u_1, u_2	axial and radial velocity components
$\overline{u_i' u_j'}$	turbulent stresses
$\hat{W}$	source terms of turbulent transport equations
x_1, x_2	axial and radial co-ordinates
y^+	dimensionless normal distance from solid wall

Greek letters

ε	turbulent dissipation rate
ξ, η	transformed co-ordinates
ρ	density

Subscripts

∞	freestream value
l	laminar
t	turbulent
v	viscous

REFERENCES

1. R. M. Beam and R. F. Warming, 'An implicit factored scheme for the compressible Navier–Stokes equations', *AIAA J.*, **16**, 393–402 (1978).
2. L. B. Wigton, N. J. Yu and D. P. Young, 'GMRES acceleration of computational fluid dynamic codes', *AIAA Paper 85-1494CP*, 1985.
3. S. Obayashi, 'Numerical simulation of underexpanded plumes using upwind algorithms', *AIAA Paper 88-4360*, 1988.
4. P. Sonneveld, 'CGS, a fast Lanczos-type solver for nonsymmetric linear systems, *SIAM J. Sci. Stat. Comput.*, **10**, 36–52 (1989).
5. Y. Saad and M. Schultz, 'GMRES: a generalized minimum residual algorithm for solving nonsymmetric linear systems', *SIAM J. Sci. Stat. Comput.*, **7**, 856–869 (1986).
6. H. A. Van Der Horst, 'Bi-CGSTAB: a fast and smoothly converging variant of Bi-CG for the solution of nonsymmetric linear systems', *SIAM J. Sci. Stat. Comput.*, **13**, 631–644 (1992).
7. R. W. Freund, 'A transpose-free quasi-minimal residual algorithm for non-Hermitian linear systems', *SIAM J. Sci. Stat. Comput.*, in press.
8. V. Venkatakrishnan, 'Preconditioned conjugate gradient methods for the compressible Navier–Stokes equations', *AIAA J.*, **29**, 1092–1100 (1991).
9. K. Ajmani, W.-F. Ng and M.-S. Liou, 'Generalized conjugate–gradient methods for the Navier–Stokes equations', *AIAA Paper 91–1556*, 1991.
10. H. Lin, D. Y. Yang and C. C. Chieng, 'Variant bi-conjugate gradient methods for compressible Navier–Stokes solver with a two-equation model of turbulence', *AIAA Paper 93–3316*, 1993.
11. T. A. Meijerink and H. A. van der Vorst, 'Guidelines for the usage of incomplete decompositions in solving sets of linear equations as they occur in practical problems', *J. Comput. Phys.*, **44**, 134–155 (1981).
12. D. A. Johnson, C. C. Horstman and W. D. Bachalo, 'Comparison between experiment and prediction for a transonic turbulent separated flow', *AIAA J.*, **20**, 737–744 (1982).

13. W. D. Bachalo and D. A. Johnson, 'Transonic, turbulent boundary-layer separation generated on an axisymmetric flow model', *AIAA J.*, **24**, 437–443 (1986).
14. C. C. Horstman, G. S. Settles, S. M. Bogdonoff and C. M. Hung, 'Reynolds number effects on shock-wave turbulent boundary-layer interactions', *AIAA J.*, **15**, 1152–1158 (1977).
15. D. S. Dolling and M. T. Murphy, 'Unsteadiness of the separation shock wave structure in a supersonic compression ramp flowfield', *AIAA J.*, **21**, 1628–1634 (1983).
16. J. L. Herrin and J. C. Dutton, 'An experimental investigation of the supersonic axisymmetric base flow behind a cylindric afterbody', *UILU 91-4004*, 1991.
17. J. L. Herrin and J. C. Dutton, 'Supersonic base flow experiments in the near-wake of a cylindrical afterbody', *AIAA Paper 93-2924*, 1993.
18. N. Shima, 'A Reynolds-stress model for near-wall and low-Reynolds-number regions', *J. Fluids Eng.*, **110**, 38–44 (1988).
19. H. C. Yee and A. Harten, 'Implicit TVD scheme for hyperbolic conservation laws in curvilinear coordinates', *AIAA Paper 85-1513*, 1985.
20. S. R. Chakravarthy, 'Relaxation methods for unfactored implicit schemes', *AIAA Paper 84-0165*, 1984.
21. R. W. MacCormack, 'Current status of numerical solutions of the Navier–Stokes equations', *AIAA Paper 85-0032*, 1985.
22. R. Fletcher, 'Conjugate gradient methods for indefinite systems', in *Lecture Notes in Mathematics*, Vol. 506, Springer, Berlin 1976, pp. 73–89.
23. R. W. Freund and N. M. Nachtigal, 'QMR: a quasi-minimal residual method for non-Hermitian linear systems', *Numer. Math.*, **60**, 315–339 (1991).
24. A. J. Peace, 'Turbulent flow predictions for afterbody/nozzle geometries including base effects', *J. Propuls.*, **7**, 396–403 (1991).
25. Y. Matsuo and W. J. Chyu, 'Computations of separated aerodynamic flows using a low Reynolds number k–ε model', *Proc. 5th Int. Symp. on Computational Fluid Dynamics*, Sendai, 1993, Vol. 2, pp. 206–211.
26. D. A. Johnson, 'Transonic separated flow predictions with an eddy-viscosity/Reynolds-stress closure model', *AIAA J.*, **25**, 252–259 (1987).
27. U. C. Goldberg and S. R. Chakravarthy, 'Prediction of separated flows with a new backflow turbulence model', *AIAA J.*, **26**, 405–408 (1988).
28. C. C. Chuang and C. C. Chieng, 'Navier Stokes computations for turbulent transonic projectile with a two-layer model combining the ASM model of turbulence and the k–ε model near the wall', *AIAA Paper 92-0518*, 1992.
29. T. J. Coakley and P. G. Huang, 'Turbulence modeling for high speed flows', *AIAA Paper 92-0436*, 1992.
30. U. C. Goldberg and S. R. Chakravarthy, 'Separated flow predictions using a hybrid k–L/backflow model', *AIAA J.*, **28**, 1005–1009 (1990).
31. C. C. Chuang and C. C. Chieng, 'Supersonic base flow computation by higher order turbulence models', *Proc. Int. Symp. on Turbulence, Heat and Mass Transfer*, Lisbon, August 1994.